Direct Experimental Evidence of Metal-Mediated Etching of Suspended Graphene

Quentin M. Ramasse,[†,*] Recep Zan,[‡,§] Ursel Bangert,[§] Danil W. Boukhvalov,[⊥] Young-Woo Son,[⊥] and Konstantin S. Novoselov[‡]

[†]SuperSTEM Laboratory, STFC Daresbury Campus, Daresbury WA4 4AD, United Kingdom, [‡]School of Physics and Astronomy and [§]School of Materials, The University of Manchester, Manchester, M13 9PL, United Kingdom, and [⊥]School of Computational Sciences, Korea Institute for Advanced Study, Seoul 130-722, Korea. The first two authors have contributed equally to the work.

ABSTRACT

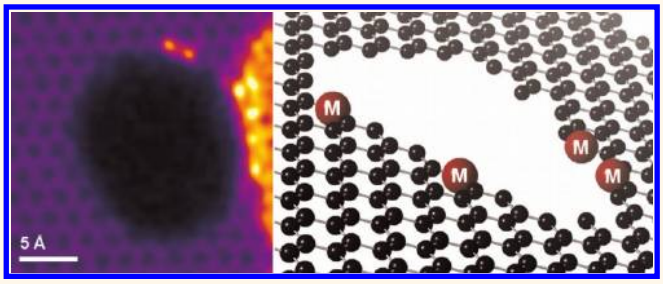

Atomic resolution high angle annular dark field imaging of suspended, single-layer graphene, onto which the metals Cr, Ti, Pd, Ni, Al, and Au atoms had been deposited, was carried out in an aberration-corrected scanning transmission electron microscope. In combination with electron energy loss spectroscopy, employed to identify individual impurity atoms, it was shown that nanoscale holes were etched into graphene, initiated at sites where single atoms of all the metal species except for gold come into close contact with the graphene. The e-beam scanning process is instrumental in promoting metal atoms from clusters formed during the original metal deposition process onto the clean graphene surface, where they initiate the hole-forming process. Our observations are discussed in the light of calculations in the literature, predicting a much lowered vacancy formation in graphene when metal ad-atoms are present. The requirement and importance of oxygen atoms in this process, although not predicted by such previous calculations, is also discussed, following our observations of hole formation in pristine graphene in the presence of Si-impurity atoms, supported by new calculations which predict a dramatic decrease of the vacancy formation energy, when SiO_x molecules are present.

KEYWORDS: graphene · scanning transmission electron microscopy · EELS · dopants · single atoms · etching

Since the first isolation of single layer graphite,[1] or graphene, a large body of research has been devoted to the remarkable electronic, structural, and physical properties of this unique material, often with a view to utilizing it for practical applications.[2] Almost by definition, however, the fabrication of any graphene-based device involves the incorporation of metal contacts, to exploit its thermal or electrical conductivity for instance. The use of either Au, Cr, Ti, or Pd has been shown to dramatically affect the performance of the resulting devices, and it follows that the choice of metal is therefore key to a successful design.[3,4] Furthermore, metals like Zn,[5] Ni,[6,7] Ag,[8,9] and Co[10,11] or even nonmetallic SiO_x[12] have all been used to tailor graphite and graphene into specific shapes such as nanoribbons, by either oxidation or hydrogenation at elevated temperature, resulting in the formation of various byproducts.[13] As a result, a number of recent studies have focused on the behavior and interactions of deposited metal ad-atoms or nanoparticles on graphene surfaces. Most of these are based on theoretical simulations such as Monte Carlo, molecular dynamics (MD) or density functional theory (DFT) to calculate the structure, bonding, and potential charge transfer of different adsorbed metal ad-atoms on materials.[14−18] Unfortunately, depending on the approach used for these calculations and in particular the choice of parameters and approximations, the results are not always consistent. Ni, for instance, was predicted to exhibit either strong[16,19] or weak[18,20] binding to graphene. As a general rule, however, transition metals (TM) have been predicted to bond covalently to the graphene surface resulting in significant lattice distortions while by contrast alkaline metals are ionically bonded to graphene and cause little distortion.[14,21] In practice, it was recently demonstrated experimentally that instead of adhering to the free surface of graphene metals tend to cluster on top of the ubiquitous hydrocarbon-based contamination, which seems to indicate a very weak affinity between metals and graphene.[22] This weak TM−graphene interaction can be mediated by deliberately introducing vacancies (*i.e.*,

* Address correspondence to qmramasse@superstem.ac.uk.

Received for review January 31, 2012 and accepted April 24, 2012.

Published online April 24, 2012
10.1021/nn300452y

defective sites) into graphene sheets prior to deposition where some metal atoms can then be trapped[23−25] as a result of bonding rearrangements around the defects and a decrease of the adsorption energy barrier. In this case, it was recently calculated that with the exception of Au, whose interaction with graphene is consistently predicted to be weak, the presence of Al, Fe, Co, and Ni metal atom impurities on or within the graphene layer can in turn lead to a dramatic reduction of the formation energies of further defects and therefore to the formation of large holes in the sheet. This would imply that graphene could be destroyed easily by the mere addition of metal atoms, a conclusion that has serious potential implications for graphene device fabrication.[26] It is therefore essential to devote renewed experimental attention to metal−graphene interactions in order to confirm or disprove this predicted deleterious behavior and perhaps to propose new mechanisms whereby it could be alleviated. Transmission electron microscopy (TEM) is the ideal tool for such studies, especially with the mounting interest in so-called suspended devices, which eliminate substrate effects and thus exploit the intrinsic properties of free-standing graphene.[2] Indeed, the technique's ability to image and identify directly each and every atom in 2D materials has already played a significant role in the establishment of graphene as one of the most studied materials of the 21st century by providing arguably the most visually striking proofs of its existence.[27]

Here we present a systematic scanning transmission electron microscopy (STEM) study of the interaction of suspended single-layer graphene sheets with metals, namely Au, Cr, Ti, Pd, Ni and Al, as well as with Si (present in our samples as an unintentional impurity: see Materials and Methods), through a model system consisting of individual ad-atoms and/or aggregates of atoms (clusters) deposited on free-standing graphene. The effects on the structure of graphene were observed at ambient temperature in ultra-high-vacuum ($<5 \times 10^{-9}$ Torr) and at a primary beam energy (60 keV) well below the knock-on damage threshold for carbon,[28] that is, in conditions that are expected to allow for safe, prolonged, observation of the material without altering its structural integrity. A combination of chemically sensitive Z-contrast imaging and electron energy loss spectroscopy (EELS) allowed us to confirm that despite these specific environmental conditions, etching does take place in the presence of all deposited elements with the exception of Au. Etching systematically initiated at the edges between clean graphene areas and the macro-molecular contamination layers where the metal clusters and impurity atoms tend to sit. On the basis of further theoretical results, we suggest that this behavior is due to the local oxidation of the metallic ad-atoms, the oxygen activation energy barrier being possibly overcome by local heating as a result of energy transfer from the beam followed by C-atom dissociation through C−O formation.

Although only on a model system, the observation and elucidation of this metal-mediated etching behavior is an essential result at a time when graphene is moving from the laboratory to the factory floor. A better understanding of the properties of metal contacts on suspended single layer graphene is essential for device fabrication, patterning, and improving performance, and our results point to the need for more systematic studies of nucleation and coverage in order to determine optimal contacts.[3,4]

RESULTS AND DISCUSSIONS

The monolayer graphene sheets used for this study were grown by chemical vapor deposition (CVD) on a copper substrate according to the method described by Li *et al.*,[29] and metals were introduced onto the graphene membranes by means of evaporation, prior to STEM measurements. Figure 1 shows low magnification HAADF images of Au (a), Cr (b), Ti (c), Pd (d), Ni (e), and Al (f) deposited on single layer graphene sheets (as verified using electron diffraction in a conventional TEM prior to deposition: see Supporting Information, Figure S1). The same amount of metal (2 Å) was evaporated in each case for accurate comparison. Consistent with recent observations, the deposited metals have formed clusters located exclusively on top of the ubiquitous hydrocarbon contamination (residues from the transfer, or contamination due to exposure to air) partially covering the surface of graphene.[22] No such clusters were observed directly on clean single-layer graphene (the darker patches on Figure 1) throughout this study, irrespective of the preparation method. A similar amount of Au was deposited on exfoliated single layer graphene (not shown here) resulting in a similar behavior to the CVD-grown samples, on which we will concentrate for the rest of this study. This lack of adherence of transition metal atoms on pure graphene, or in other words their apparent high mobility on clean graphene surfaces, illustrates how significantly stronger the metal−metal interactions are than the metal−graphene interactions.[22,30] Indeed this behavior was predicted by DFT calculations[31] and MD simulations,[32] which suggested that clustering is more energetically favorable than remaining isolated for transition metal atoms. By contrast alkali metals are expected to form 2-dimensional continuous films on top of the graphene surface.[32]

Despite identical deposition conditions the physiognomy of the samples varies significantly. Au clusters (Figure 1a) are larger and denser and as a result coverage is sparser than for the other metals. Pd (Figure 1d) and Ni (Figure 1e) also agglomerate into well-defined metallic nanoparticles, albeit of much smaller sizes than Au, resulting in a more uniform

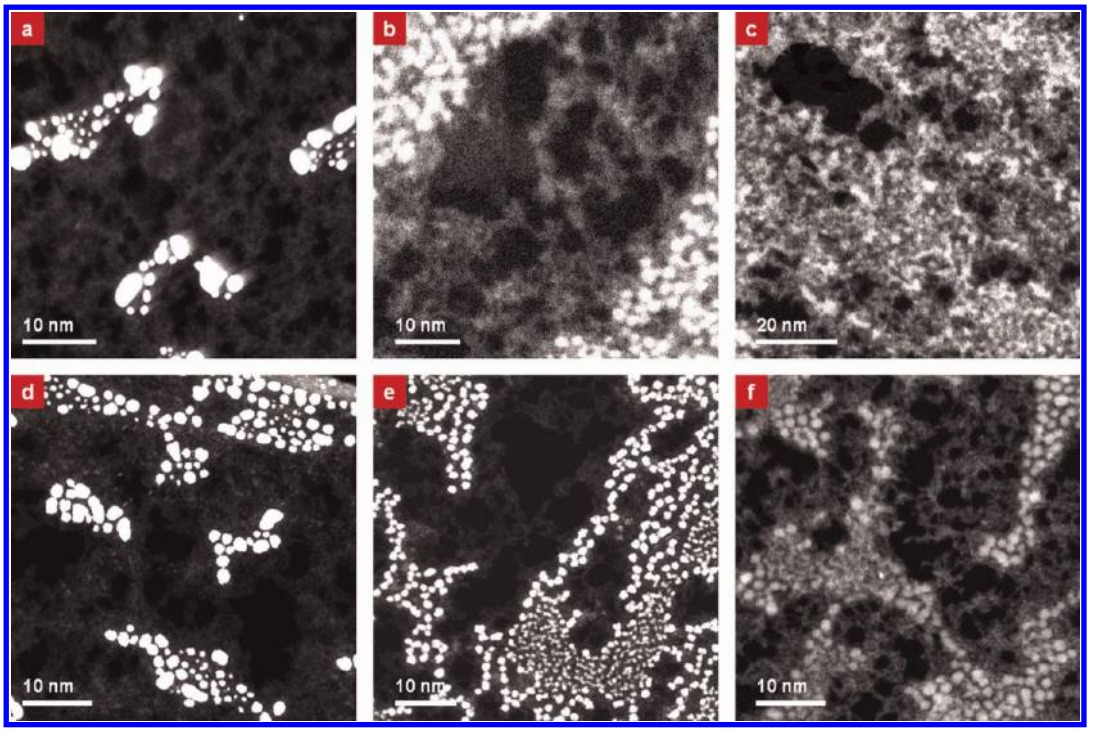

Figure 1. Low magnification HAADF images of metals on monolayer graphene show an overview of the metal distribution for (a) Au, (b) Cr, (c) Ti, (d) Pd, (e) Ni, and (f) Al. The contrast and intensity were adjusted to reveal areas of clean graphene (dark patches) and "contamination" layers (light gray patches) where the metals (white clusters) sit preferentially.

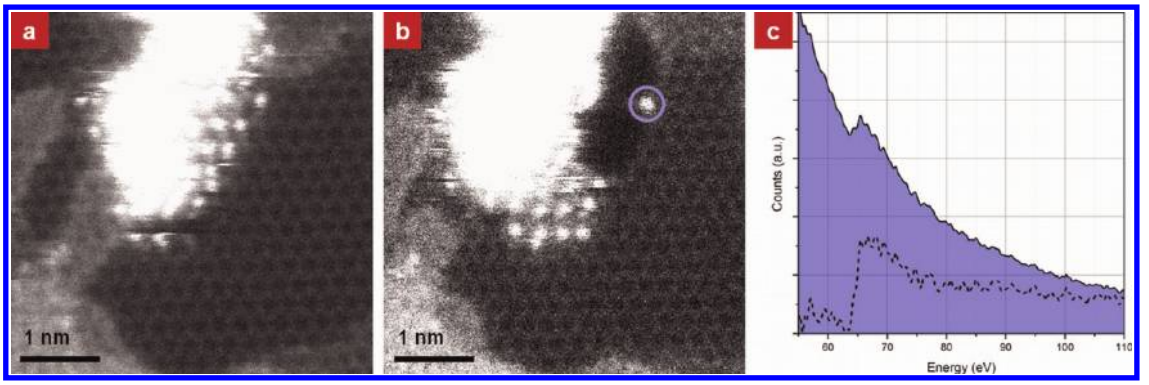

Figure 2. (a) HAADF image of a Ni cluster sitting on the very edge of the hydrocarbon contamination layer. Single Ni atoms have been dragged by the beam from the cluster and are in contact with the graphene monolayer. (b) After a few more scans, a hole has formed, whose edges are decorated by single Ni atoms, identified by their Ni $M_{2,3}$ EELS signal. (c) EELS spectrum acquired by positioning the beam for 1 s on the bright atom circled in image b.

coverage of the sample. Cr (Figure 1b) and particularly Ti (Figure 1c) and Al (Figure 1f) exhibit a much higher fractional coverage with loose, flat, atomic aggregates.

The propensity of the latter to oxidize into alumina may explain the aspect of that particular sample as the deposited Al may have oxidized during sample transport from the deposition chamber to the microscope or upon contact with the hydrocarbon layer. A similar argument can be made for Ti and Cr, which are commonly used as a precursor for the fabrication of Au contacts on graphene: the better coverage of the sample after deposition of those two metals observed here may be an illustration of their effectiveness for such applications. Although none were applied here, surface pretreatments such as hydrogenation (or oxidation) have been shown to affect the adherence of metals to the samples, resulting for instance in smaller Au clusters and a more uniform coverage which in turn is easily degraded by beam-induced coalescence of the clusters under the electron beam.[30]

Although as can be seen in the overview images of Figure 1, the metal clusters sit preferentially in the middle of the hydrocarbon contamination, after a few scans of the electron beam at mid- to high-resolution (for high signal-to-noise images each scan can take up to 30 s), some of the clusters and/or individual atoms can be dragged by the beam to the edge of the contamination layer. Figure 2a shows an HAADF image

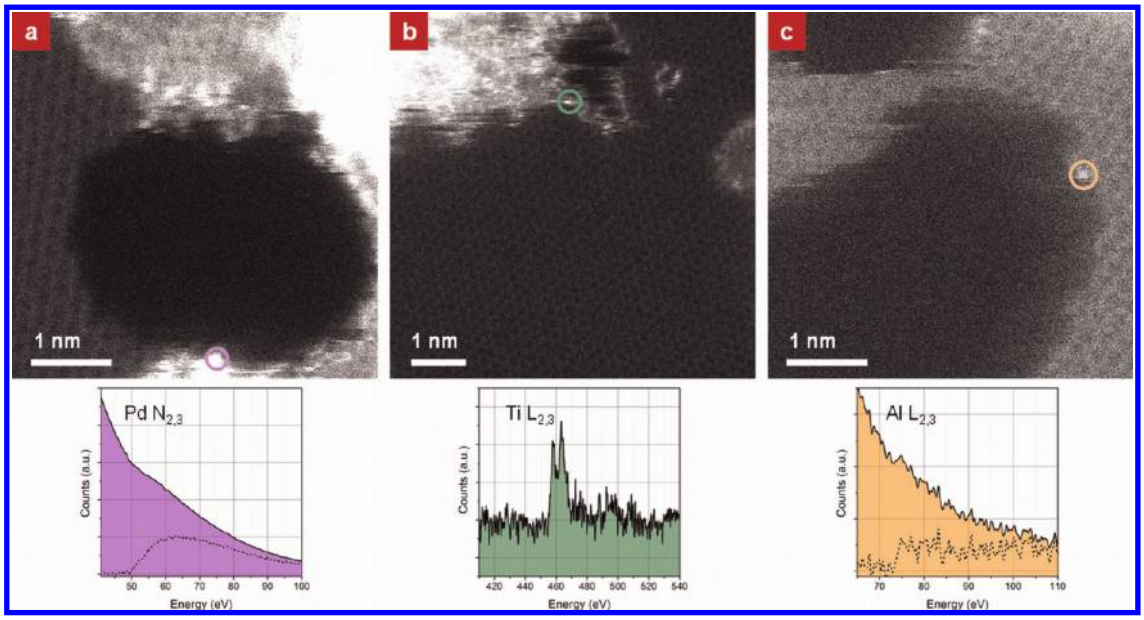

Figure 3. HAADF images of holes formed in monolayer graphene through metal-mediated etching for (a) Pd, (b) Ti, and (c) Al. EELS spectra acquired by positioning the beam for 1 s on the atoms circled on the images are shown below. The dotted lines correspond to the EELS signal after background subtraction with a power law.

of such a Ni cluster positioned at the very edge of a contamination area. Individual Ni atoms can be also seen to form a raft above a region of clean single layer graphene at the edge of the particle. While some carbon chains may still be present immediately under these Ni atoms, such a configuration offers a great proximity between pure graphene and the metal atoms. After a few additional scans of the beam, a hole has formed (Figure 2b), decorated by individual Ni atoms as evidenced by the clear Ni $M_{2,3}$ signature in the EEL spectrum (Figure 2c), acquired by placing the electron probe exactly on top of the bright atom marked on Figure 2b. This hole formation is obviously dynamic and additional stills from a time series of over 90 consecutive images illustrate the process further (see Supporting Information, Figure S2). After the initial hole formation, individual Ni atoms are observed to jump onto the exposed edge before the hole is further enlarged, producing bright horizontal streaks in the images (Figure 2a) as they are being captured at different positions by the beam as it is being rastered in a line. They can only be imaged once in a more stable position at the edge of the hole, such as on Figure 2b. A strong indication that the drilling process is indeed metal-mediated arises from the observation that when no Ni atom is decorating the hole, the latter merely reshapes dynamically (as expected from earlier reports[33]) but does not grow further in size (see Supporting Information, Figure S3). In other words, the drilling stabilizes when the local reservoir of metal impurity atoms is exhausted and until more Ni atoms are drawn toward the energetically unstable edges of the hole *via* surface diffusion thanks to the high mobility of single metal impurities on single layer graphene.

This behavior (migration of the metal atoms under the beam to the edge of the contamination layer, drilling, and hole enlargement) was reproduced identically when imaging single-layer graphene samples on which palladium (Figure 3a), titanium (Figure 3b), and aluminum (Figure 3c) had been deposited, while in an earlier report a similar process had probably been at play but not recognized for the interaction of Cr with graphene.[22] In each case, the nature of the atoms decorating the edges of the newly formed holes was confirmed by placing the electron probe directly on top of them and recording an EELS spectrum, as shown on Figure 3.

Metals have been used as catalysts for patterning of graphene devices in hydrogen or oxygen flow at high temperatures,[6,9,11] and the addition of Ni in particular was predicted to lead to very low defect formation energies when interacting with single layer graphene.[26] However, neither gas environment nor high temperatures were used in our study, which is to our knowledge the first experimental evidence of electron beam-induced drilling of graphene through its direct interaction with metals. D. W. Boukhvalov and M. I. Katsnelson predicted this destructive behavior (specifically for Fe, Co, Ni, and Al) by calculating a drastic lowering of the formation energy for mono- and divacancies in single layer graphene when metal ad-atoms are present on the graphene surface.[26] The precise mechanism they propose in their *ab initio* calculations assumes a direct contact between a metal atom and the surface of free-standing graphene before the formation of the defects: as noticed above, some direct contact can be observed at the very edge of the contamination layer after a few scans of the electron

beam, as illustrated on Figure 2a. While our observations seem to provide a direct experimental evidence of this metal-mediated destruction of graphene, it is important to consider other possible reasons for the severe drilling behavior we observed.

Although all are transition metals, these elements have been predicted to interact with graphene quite differently. Palladium has been used as an electrical contact in device fabrication for many years[34] and most recently in graphene devices[35] because of its lower cost compared to gold. Although it has a full d-shell, it is expected to bond covalently to graphene with a reasonably high adsorption energy.[14,19] Recent DFT calculations also suggest that Pd atoms have a strong tendency to form three-dimensional rather than planar clusters on graphene, which indicate a weak Pd−graphene interaction[36] as evidenced by our observation (see Figure 1d). Of all the metals used for this study, Ti is predicted to have the strongest interaction with graphene, bonding to its surface *via* chemisorption.[17,19] Finally, Al is predicted to have ionic bonding to the graphene surface, similarly to the case of I−III metals, which unlike transition metals[14] are not seeing a significant modification of their electronic state. Furthermore, Al-doped graphene has been shown to be a promising material for hydrogen storage[37] while the deposition of a layer of aluminum oxide can be used as a gate insulator in graphene device fabrication.[38]

A constant trait of all those elements is their propensity to form oxides, which suggests that oxidation could be playing a major role in the effects we are observing. This theory could be further strengthened by the fact that by contrast no hole-forming was observed on Au-deposited samples (see Supporting Information, Figure S4 and, for instance, Zan *et al.*[30]), Au being of course not prone to oxidation except in very specific circumstances.[39] Nevertheless, even in the monovacancy formation model for the destruction of graphene proposed by Boukhvalov *et al.*,[26] Au is not expected to lead to a major loss in stability as its defect formation energy remains high so this observation cannot definitively point to a role of O in this etching process. The depositions were conducted in thermal and e-beam evaporators where the vacuum is at least 10^{-7} Torr, all metals being degassed prior to evaporation. The most likely sources of oxygen, should any be involved in this process, are therefore: the oxidation of the metal clusters and/or the retention of O by the hydrocarbon contamination during transport of the samples from the deposition chamber to the microscope; or a relatively high partial pressure of O in the microscope column. All samples were systematically left within the microscope vacuum for several days to ensure perfect thermal and mechanical equilibrium during observation: after such long waiting periods the slight pressure increase in the column due to sample insertion had subsided and the sample chamber was systematically at its base pressure of $<5 \times 10^{-9}$ Torr. Sample degassing can be thus considered as an unlikely source of O. Graphene etching in an oxygen environment is well-documented, and the energy required for the oxidation of graphene is expected to be low.[40] Therefore, should a high partial pressure of O in the chamber be responsible for the observed hole formation it should be occurring everywhere, not only at the edges of the hydrocarbon contamination. Furthermore, at 60 kV and in otherwise identical conditions perfectly clean patches of graphene were imaged by scanning the beam repeatedly for over an hour without any drilling. The hole formation mechanism we report here must therefore be either solely metal-mediated as in the model from Boukhvalov *et al.*,[26] or involve metal adatoms and oxygen from either oxidized metal clusters or oxidized surface contamination.

As a control experiment we studied a pristine graphene sample, that is, a single layer graphene sheet produced and processed in identical conditions but on which no metal was deposited. As mentioned previously, in the conditions used for our observations pristine single layer graphene patches can be imaged without any visible damage for extremely long periods of time, and with very large electron doses. Some carbon surface contamination may occasionally diffuse into the field of view depending on the area being observed (the C support film may act as a contamination reservoir), but drilling or etching was never noticed when imaging clean areas of our samples. Although every attempt was made at obtaining extremely clean single layer graphene samples prior to metal deposition, Si contaminants, either in the form of relatively large SiO_x clusters or of small single Si atoms are common[41] and were readily observed in our samples.

Substitutional Si impurities were found to be very stable. Figure 4a shows an HAADF image of a such a Si impurity, identified by EELS by placing the beam directly on top of it (Figure 4b). Several such data sets were acquired sequentially, with the Si impurity atom always appearing on HAADF images recorded immediately after the 2s EELS acquisition took place, proof of the great stability of this structure. However, when imaging continuously the edge of a hydrocarbon contamination layer containing some Si impurities (identified by EELS), we were able to observe even on such pristine samples the formation of a hole in the graphene sheet, although not as readily as with metal-deposited samples.

As in the metal case, the edges of the thus-formed hole were subsequently decorated by single atoms (figure 4c), identified as Si atoms by EELS (figure 4d). Again, the process was observed to continue until the local reservoir of Si impurity atoms is exhausted, at which point the drilling is halted and only a dynamic reshaping of the edges of the hole can be observed under the beam.

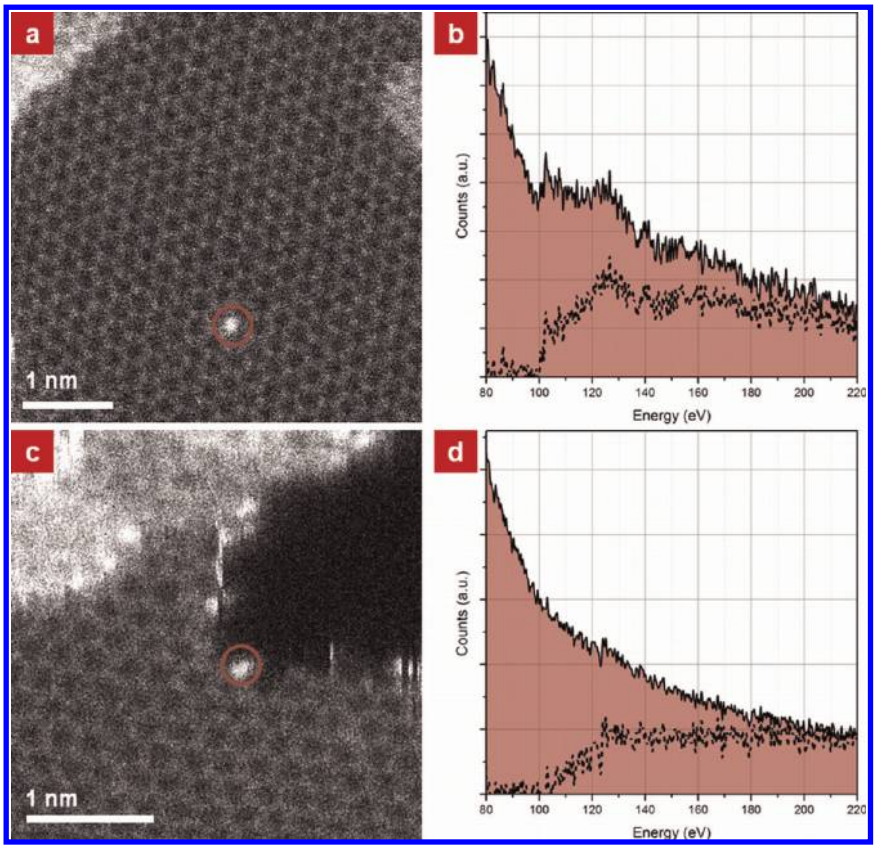

Figure 4. (a) HAADF image of a single substitutional Si atom within a graphene monolayer. An EELS point spectrum (b) acquired by positioning the beam for 1 s on the atom confirms it is Si. This defect is extremely stable as it was possible to record several successive such data sets, the atoms remaining in position throughout. (c) HAADF image and corresponding EELS point spectrum (d) of a Si atom decorating a hole, just formed at the edge of the hydrocarbon contamination layer. The signal after background subtraction with a power law model is shown as the dotted line.

SiO_x has been shown to have potential applications in tailoring graphene sheets to specific shapes during annealing in hydrogen atmosphere around 900 °C, the high temperature, high pressure environment being crucial to the production of SiO_x particles from the surface of a Si/SiO_2 wafer.[12] The present, previously unreported, drilling mechanism observed on pristine samples is therefore quite different and may depend crucially on the vacancy formation energy barrier in case of a single Si adatom, Si cluster, SiO_2 molecules and/or SiO_2 cluster. We found computationally that single Si ad-atoms and crystalline Si clusters have similar vacancy formation energies (8.33 eV and 8.36 eV, respectively). These are close to the energy required for the formation of a single vacancy in graphene by irradiation (7 eV)[42] and it can therefore be concluded that the presence of Si ad-atoms or crystalline clusters should not lead to any drilling behavior. Similarly, unpassivated quartz (ordered SiO_2) was revealed to be relatively `safe'' for graphene: the energy required for the migration of a single oxygen from SiO_2 to the graphene surface is 3.14 eV (much higher than the energy required for the oxidation of graphene reported in the literature), while the unzipping of graphene along defect lines of carbon monoxide molecules[43] is unlikely as the required energies for a single and a pair of epoxy groups are 6.94 and 9.69 eV, respectively. On the other hand, disordered silicon oxide molecules and clusters provide a plausible solution as both have a tendency to form metastable intermediate $Si_xO_yC_z$ structures.[44] The energies required for this process are 3.13 and 2.46 eV for silicon oxide molecules and silicon oxide clusters, respectively, which are very much comparable to the 2.5 eV energy formation of a monovacancy in the presence of Ni[26] (see Supporting Information for details on the modeling parameters, Figure S5). We therefore propose that as in the case of metal-deposited graphene, disordered SiO_x molecules find themselves dragged to the edge of the contamination layer, where they interact with the graphene sheet. Upon formation of an initial unstable $Si_xO_yC_z$ structure, as suggested by our calculations, a hole appears and grows through the same mechanism, Si atoms or SiO_x clusters being drawn energetically to the exposed edges.

Finally, we point out that the exact role of the electron beam in either the metal-mediated drilling or in the Si case could not be directly elucidated from our sole observations. However, the formation of holes at the edge of the contamination layers away from the region being imaged (up to tens of nm) and the

excellent conduction properties of graphene[45] point to a heat transfer mechanism, whereby local heating as a result of the irradiation by the beam is sufficient to overcome the defect formation energy barriers.

CONCLUSIONS

Using atomic resolution HAADF imaging and identification of single atoms by EELS, we have observed etching of suspended, single-layer graphene upon which metal atoms had been deposited. Etching occurred with all employed metals (Cr, Ti, Pd, Ni, and Al) apart from gold. It also occurred in pristine samples with (unintentional) Si contamination. Metal clusters nucleate initially exclusively on hydrocarbon contamination. Nanoscale holes form in locations where metal atom clusters sit at the border of the contamination with pristine graphene, following the drag of individual metal atoms onto the pristine graphene surface during the e-beam scan. Theoretical modeling predicts that vacancy formation energies in graphene are substantially lowered in the presence of metal atoms. Although according to such calculations the presence of oxygen is not required in this metal-mediated vacancy formation, we suggest oxygen is present and indeed assists C−C bond dissociation *via* graphene oxidation. We derive this from the fact that vacancy formation in the presence of Si-oxide has much lower predicted energies—similar to these calculated for vacancy formation in the presence of Ni- than for Si-atoms or Si-clusters alone. The presence of O is further indicated by the fact that holes form at the edges of hydrocarbon contamination, added to observations that atoms from the deposits are being dragged onto the clean graphene. Lastly, etching does not occur in the presence of gold atoms, which do not oxidize, although the predicted vacancy formation energy is lowered. The role of the scanning electron probe is not fully established, but since hole formation also occurred in regions adjacent to but not directly in the e-beam scanned area, we suggest that the e-beam acts as a heat source.

MATERIALS AND METHODS

The monolayer CVD grown graphene membranes were transferred to the TEM support grids using a standard wet chemistry methodology. Conventional TEM was used to the assess the quality of the produced films: electron diffraction data confirmed near perfect coverage of the entire TEM grids with a single layer graphene sheet.[46] The samples were then placed either into an electron beam evaporator (for depositing Au, Cr, Ti, and Pd) or a thermal evaporator (for depositing Al and Ni). In all cases, the same amount of material (2 Å of Au, Cr, Ti, Pd, Ni and Al) was deposited with a precisely calibrated rate of 0.1 Å/s, in a custom-made deposition chamber whose pressure ranged from 10^{-6} to 10^{-8} Torr during the evaporation. While Si atoms were not introduced deliberately, they were consistently observed as a widely present contaminant both on metal-deposited samples and on pristine graphene samples. The presence of Si (and SiO_x) contaminants on graphene has been widely reported for both CVD-grown and exfoliated graphene.[41] The support films, another possible origin for the Si contaminants, were all but ruled out as a source in our case: Si single atoms and SiO_x clusters were indeed consistently observed on as-prepared pristine graphene samples transferred onto different types of support grids (lacey carbon film, holey carbon film, and Quantifoil) purchased from different suppliers.

All electron micrographs were acquired at the SuperSTEM Laboratory on a Nion UltraSTEM100 dedicated scanning transmission electron microscope equipped with a cold field emission gun with a native energy spread of 0.35 eV and operated at 60 kV to prevent knock-on damage to the graphene samples. This instrument has an ultra-high-vacuum (UHV) design throughout, allowing pressures at the sample of below 5×10^{-9} Torr. The beam was set up to a convergence semiangle of 30 mrad with an estimated beam current of 45 pA at the sample. In these operating conditions the estimated probe size is 1.1 Å. The high angle annular dark field (HAADF) detector used to record the Z-contrast images had inner and outer radii of 86 and 190 mrad respectively. Detectors with lower inner angles (medium and low angle annular dark field detectors, MAADF and LAADF) can provide an increased signal-to-noise in images of low atomic number materials while retaining good signal interpretability for ultrathin samples (there is no dynamical effect for samples one atom thick) and they have been used recently to great effect for atom-by-atom chemical analysis.[47] As this study is concerned with impurity atoms deposited on top of the graphene samples, HAADF imaging was used throughout to avoid potential nonlinearity effects in MAADF images, thus retaining the approximate Z^2-dependence of the imaging process whereby the intensity recorded with the probe positioned on an atomic site is approximately proportional to the square of the average atomic number Z of this site.[47] Electron energy loss spectra were recorded on a Gatan Enfina spectrometer with acquisition times between 1 and 2 s (as specified in the text) for point spectra. The spectrometer acceptance semiangle was calibrated at 33 mrad.

Interactions between graphene and silicon adatom (clusters) or Si_xO_y clusters were further studied using a first-principles calculation method implemented in the SIESTA code,[48] as was done in previous work.[25,26,40] In modeling these interactions, the generalized gradient approximation (GGA-PBE)[49] was adopted to describe the exchange-correlation energy, which has been used in understanding graphene destruction[26] and oxidation.[25,40] Another theoretical consideration is the interaction between graphene and a quartz substrate. In this case, the local density approximation (LDA)[50] instead of the GGA-PBE is used because the latter fails to describe the weak graphene−substrate interactions.[51] The atomic positions were fully relaxed within the maximum force of 0.04 eV/Å on individual atoms. The ion cores are described by norm-conserving nonrelativistic pseudopotentials[52] with cut off radii 1.90, 1.15, and 1.25 au for Si, O, and C, respectively, and the wave functions are expanded with localized atomic orbitals (a double-ζ plus polarization basis set). All calculations were carried out with an energy mesh cutoff of 360 Ry. We used a rectangular shaped supercell containing 48 carbon atoms to model interactions between graphene and silicon atoms or clusters.[40] For the modeling of the interaction of graphene with an unpassivated quartz (ordered SiO_2) surface we used a graphene supercell containing 32 carbon atoms over 9 Si atomic layers of α-quartz previously used in ref 51. For these two models we used the k-point mesh of $8 \times 6 \times 1$ and $4 \times 4 \times 1$ in the Monkhorst−Pack scheme,[53] respectively.

Conflict of Interest: The authors declare no competing financial interest.

Acknowledgment. This work was supported by the EPSRC (UK). We acknowledge computational support from the CAC of KIAS. Y.-W. S. was supported by the NRF grant funded by the

government of Korea, MEST (Quantum Metamaterials Research Center, R11-2008-053-01002-0).

Supporting Information Available: Details about the sample screening procedure, additional images of the etching process, and a detailed description of the modeling parameters and assumptions used for the *ab initio* calculations. This material is available free of charge *via* the Internet at http://pubs.acs.org.

REFERENCES AND NOTES

1. Novoselov, K. S.; Geim, A. K.; Morozov, S. V.; Jiang, D.; Zhang, Y.; Dubonos, S. V.; Grigorieva, I. V.; Firsov, A. A. Electric Field Effect in Atomically Thin Carbon Films. *Science* **2004**, *306*, 666–669.
2. Ponomarenko, L. A.; Geim, A. K.; Zhukov, A. A.; Jalil, R.; Morozov, S. V.; Novoselov, K. S.; Grigorieva, I. V.; Hill, E. H.; Cheianov, V. V.; Falko, V. I.; *et al*. Tunable Metal-Insulator Transition in Double-Layer Graphene Heterostructures. *Nat. Phys.* **2011**, *7*, 958–961.
3. Pi, K.; McCreary, K. M.; Bao, W.; Han, W.; Chiang, Y. F.; Li, Y.; Tsai, S. W.; Lau, C. N.; Kawakami, R. K. Electronic Doping and Scattering by Transition Metals on Graphene. *Phys. Rev. B* **2009**, *80*, 075406.
4. Venugopal, A.; Colombo, L.; Vogel, E. M. Contact Resistance in Few and Multilayer Graphene Devices. *Appl. Phys. Lett.* **2010**, *96*, 013512.
5. Dimiev, A.; Kosynkin, D. V.; Sinitskii, A.; Slesarev, A.; Sun, Z.; Tour, J. M. Layer-by-Layer Removal of Graphene for Device Patterning. *Science* **2011**, *331*, 1168–1172.
6. Campos, L. C.; Manfrinato, V. R.; Sanchez-Yamagishi, J. D.; Kong, J.; Jarillo-Herrero, P. Anisotropic Etching and Nanoribbon Formation in Single-Layer Graphene. *Nano Lett.* **2009**, *9*, 2600–2604.
7. Ci, L.; Xu, Z.; Wang, L.; Gao, W.; Ding, F.; Kelly, K.; Yakobson, B.; Ajayan, P. Controlled Nanocutting of Graphene. *Nano Res.* **2008**, *1*, 116–122.
8. Booth, T. J.; Pizzocchero, F.; Andersen, H.; Hansen, T. W.; Wagner, J. B.; Jinschek, J. R.; Dunin-Borkowski, R. E.; Hansen, O.; Boggild, P. Discrete Dynamics of Nanoparticle Channelling in Suspended Graphene. *Nano Lett.* **2011**, *11*, 2689–2692.
9. Severin, N.; Kirstein, S.; Sokolov, I. M.; Rabe, J. P. Rapid Trench Channeling of Graphenes with Catalytic Silver Nanoparticles. *Nano Lett.* **2008**, *9*, 457–461.
10. Schaffel, F.; Warner, J.; Bachmatiuk, A.; Rellinghaus, B.; Buchner, B.; Schultz, L.; Rummeli, M. Shedding Light on the Crystallographic Etching of Multi-layer Graphene at the Atomic Scale. *Nano Res.* **2009**, *2*, 695–705.
11. Schaffel, F.; Wilson, M.; Bachmatiuk, A.; Rummeli, M. H.; Queitsch, U.; Rellinghaus, B.; Briggs, G. A. D.; Warner, J. H. Atomic Resolution Imaging of the Edges of Catalytically Etched Suspended Few-Layer Graphene. *ACS Nano* **2011**, *5*, 1975–1983.
12. Gao, L.; Ren, W.; Liu, B.; Wu, Z.-S.; Jiang, C.; Cheng, H.-M. Crystallographic Tailoring of Graphene by Nonmetal SiOx Nanoparticles. *J. Am. Chem. Soc.* **2009**, *131*, 13934–13936.
13. Biró, L. P.; Lambin, P. Nanopatterning of Graphene with Crystallographic Orientation Control. *Carbon* **2010**, *48*, 2677–2689.
14. Chan, K. T.; Neaton, J. B.; Cohen, M. L. First-Principles Study of Metal Adatom Adsorption on Graphene. *Phys. Rev. B* **2008**, *77*, 235430.
15. Sevincli, H.; Topsakal, M.; Durgun, E.; Ciraci, S. Electronic and Magnetic Properties of 3d Transition-Metal Atom Adsorbed Graphene and Graphene Nanoribbons. *Phys. Rev. B* **2008**, *77*, 195434.
16. Giovannetti, G.; Khomyakov, P. A.; Brocks, G.; Karpan, V. M.; van den Brink, J.; Kelly, P. J. Doping Graphene with Metal Contacts. *Phys. Rev. Lett.* **2008**, *101*, 026803.
17. Gong, C.; Geunsik, Lee; Shan, B.; Vogel, E., M.; Wallace, R. M.; Cho, K. First-Principles Study of Metal–Graphene Interfaces. *J. Appl. Phys.* **2010**, *108*, 123711.
18. Vanin, M.; Mortensen, J. J.; Kelkkanen, A. K.; Garcia-Lastra, J. M.; Thygesen, K. S.; Jacobsen, K. W. Graphene on Metals: A van der Waals Density Functional Study. *Phys. Rev. B* **2010**, *81*, 081408.
19. Yazyev, O. V.; Pasquarello, A. Metal Adatoms on Graphene and Hexagonal Boron Nitride: Towards Rational Design of Self-Assembly Templates. *Phys. Rev. B* **2010**, *82*, 045407.
20. Zólyomi, V.; Rusznyák, Á.; Koltai, J.; Kürti, J.; Lambert, C. J. Functionalization of Graphene with Transition Metals. *Phys. Status Solidi B* **2010**, *247*, 2920–2923.
21. Liu, X.; Wang, C. Z.; Yao, Y. X.; Lu, W. C.; Hupalo, M.; Tringides, M. C.; Ho, K. M. Bonding and Charge Transfer by Metal Adatom Adsorption on Graphene. *Phys. Rev. B* **2011**, *83*, 235411.
22. Zan, R.; Bangert, U.; Ramasse, Q.; Novoselov, K. S. Metal–Graphene Interaction Studied *via* Atomic Resolution Scanning Transmission Electron Microscopy. *Nano Lett.* **2011**, *11*, 1087–1092.
23. Krasheninnikov, A. V.; Lehtinen, P. O.; Foster, A. S.; Pyykko, P.; Nieminen, R. M. Embedding Transition-Metal Atoms in Graphene: Structure, Bonding, and Magnetism. *Phys. Rev. Lett.* **2009**, *102*, 126807.
24. Okamoto, Y. Density-Functional Calculations of Icosahedral M13 (M = Pt and Au) Clusters on Graphene Sheets and Flakes. *Chem. Phys. Lett.* **2006**, *420*, 382–386.
25. Boukhvalov, D. W.; Katsnelson, M. I. Chemical Functionalization of Graphene with Defects. *Nano Lett.* **2008**, *8*, 4373–4379.
26. Boukhvalov, D. W.; Katsnelson, M. I. Destruction of Graphene by Metal Adatoms. *Appl. Phys. Lett.* **2009**, *95*, 023109.
27. Gass, M. H.; Bangert, U.; Bleloch, A. L.; Wang, P.; Nair, R. R.; Geim, A. K. Free-Standing Graphene at Atomic Resolution. *Nat. Nanotechnol.* **2008**, *3*, 676–681.
28. Egerton, R. F.; Wang, F.; Crozier, P. A. Beam-Induced Damage to Thin Specimens in an Intense Electron Probe. *Microsc. Microanal.* **2006**, *12*, 65–71.
29. Li, X.; Cai, W.; An, J.; Kim, S.; Nah, J.; Yang, D.; Piner, R.; Velamakanni, A.; Jung, I.; Tutuc, E.; R., S.; *et al*. Large-Area Synthesis of High-Quality and Uniform Graphene Films on Copper Foils. *Science* **2009**, *324*, 1312–1314.
30. Zan, R.; Bangert, U.; Ramasse, Q.; Novoselov, K. S. Evolution of Gold Nanostructures on Graphene. *Small* **2011**, *7*, 2868–2872.
31. Akturk, U. Olcay; Tomak, M. Au_nPt_n Clusters Adsorbed on Graphene Studied by First-Principles Calculations. *Phys. Rev. B* **2009**, *80*, 085417.
32. Neek-Amal, M.; Asgari, R.; Tabar, M. R. R. The Formation of Atomic Nanoclusters on Graphene Sheets. *Nanotechnology* **2009**, *20*, 135602.
33. Girit, C. O.; Meyer, J. C.; Erni, R.; Rossell, M. D.; Kisielowski, C.; Yang, L.; Park, C.-H.; Crommie, M. F.; Cohen, M. L.; Louie, S. G.; *et al*. Graphene at the Edge: Stability and Dynamics. *Science* **2009**, *323*, 1705–1708.
34. Raub, C. J. Electroplating of Palladium for Electrical Contacts. *Platinum Met. Rev.* **1982**, *26*, 158–166.
35. Xia, F.; Perebeinos, V.; Lin, Y.-m.; Wu, Y.; Avouris, P. The Origins and Limits of Metal–Graphene Junction Resistance. *Nat. Nanotechnol.* **2011**, *6*, 179–184.
36. Cabria, I.; Lopez, M. J.; Alonso, J. A. Theoretical Study of the Transition from Planar to Three-Dimensional Structures of Palladium Clusters Supported on Graphene. *Phys. Rev. B* **2010**, *81*, 035403.
37. Ao, Z. M.; Jiang, Q.; Zhang, R. Q.; Tan, T. T.; Li, S. Al Doped Graphene: A Promising Material for Hydrogen Storage at Room Temperature. *J. Appl. Phys.* **2009**, *105*, 074307.
38. Wang, X.; Tabakman, S. M.; Dai, H. Atomic Layer Deposition of Metal Oxides on Pristine and Functionalized Graphene. *J. Am. Chem. Soc.* **2008**, *130*, 8152–8153.
39. Boyen, H. G.; Kastle, G.; Weigl, F.; Koslowski, B.; Dietrich, C.; Ziemann, P.; Spatz, J. P.; Riethmuller, S.; Hartmann, C.; Moller, M.; *et al*. Oxidation-Resistant Gold-55 Clusters. *Science* **2002**, *297*, 1533–1536.
40. Boukhvalov, D. W.; Son, Y.-W. Oxygen Reduction Reactions on Pure and Nitrogen-Doped Graphene: A First-Principles Modeling. *Nanoscale* **2012**, *4*, 417–420.

41. Zhou, W.; Prange, M.; Oxley, M.; Pantelides, S.; Pennycook, S.; Nanda, J.; Narula, C.; Idrobo, J. C. Atomic Scale Study of Point Defects in Graphene using STEM. *Microsc. Microanal.* **2011**, *17*), 1498–1499.
42. Banhart, F.; Kotakoski, J.; Krasheninnikov, A. V. Structural Defects in Graphene. *ACS Nano* **2011**, *5*, 26–41.
43. Li, J.-L.; Kudin, K. N.; McAllister, M. J.; Prud'homme, R. K.; Aksay, I. A.; Car, R. Oxygen-Driven Unzipping of Graphitic Materials. *Phys. Rev. Lett.* **2006**, *96*, 176101.
44. Tribaudino, M.; Artoni, A.; Mavris, C.; Bersani, D.; Lottici, P. P.; Belletti, D. Single-Crystal X-ray and Raman Investigation on Melanophlogite from Varano Marchesi (Parma, Italy). *Am. Mineral.* **2008**, *93*, 88–94.
45. Balandin, A. A.; Ghosh, S.; Bao, W.; Calizo, I.; Teweldebrhan, D.; Miao, F.; Lau, C. N. Superior Thermal Conductivity of Single-Layer Graphene. *Nano Lett.* **2008**, *8*, 902–907.
46. Meyer, J. C.; Geim, A. K.; Katsnelson, M. I.; Novoselov, K. S.; Obergfell, D.; Roth, S.; Girit, C.; Zettl, A. On the Roughness of Single- and Bi-layer Graphene Membranes. *Solid State Commun.* **2007**, *143*, 101–109.
47. Krivanek, O. L.; Chisholm, M. F.; Nicolosi, V.; Pennycook, T. J.; Corbin, G. J.; Dellby, N.; Murfitt, M. F.; Own, C. S.; Szilagyi, Z. S.; Oxley, M. P.; *et al*. Atom-by-Atom Structural and Chemical Analysis by Annular Dark-Field Electron Microscopy. *Nature* **2010**, *464*, 571–574.
48. Soler, J. M.; Artacho, E.; Gale, J. D.; Garcia, A.; Junquera, J.; Ordejon, P.; Sanchez-Portal, D. The SIESTA Method for *ab Initio* Order-N Materials Simulation. *J. Phys.: Condens. Matter* **2002**, *14*, 2745.
49. Perdew, J. P.; Burke, K.; Ernzerhof, M. Generalized Gradient Approximation Made Simple. *Phys. Rev. Lett.* **1996**, *77*, 3865–3868.
50. Perdew, J. P.; Zunger, A. Self-Interaction Correction to Density-Functional Approximations for Many-Electron Systems. *Phys. Rev. B* **1981**, *23*, 5048–5079.
51. Cuong, N. T.; Otani, M.; Okada, S. Semiconducting Electronic Property of Graphene Adsorbed on (0001) Surfaces of SiO_2. *Phys. Rev. Lett.* **2011**, *106*, 106801.
52. Troullier, N.; Martins, J. L. Efficient Pseudopotentials for Plane-Wave Calculations. *Phys. Rev. B* **1991**, *43*, 1993–2006.
53. Monkhorst, H. J.; Pack, J. D. Special Points for Brillouin-Zone Integrations. *Phys. Rev. B* **1976**, *13*, 5188–5192.